# Journal of Vibration and Control

http://jvc.sagepub.com


## Broad-band Viscoelastic Rotational Vibration Control for Remote Sensing Applications


Adam L. Webster and William H. Semke



*Journal of Vibration and Control* 2005; 11; 1339
DOI: 10.1177/1077546305057222



The online version of this article can be found at:
http://jvc.sagepub.com/cgi/content/abstract/11/11/1339

Published by:

http://www.sagepublications.com

**Additional services and information for *Journal of Vibration and Control* can be found at:**

**Email Alerts:** http://jvc.sagepub.com/cgi/alerts

**Subscriptions:** http://jvc.sagepub.com/subscriptions

**Reprints:** http://www.sagepub.com/journalsReprints.nav

**Permissions:** http://www.sagepub.co.uk/journalsPermissions.nav

**Citations** http://jvc.sagepub.com/cgi/content/refs/11/11/1339

Downloaded from http://jvc.sagepub.com at ROCHESTER INST OF TECHNOLOGY on February 4, 2009

# Broad-band Viscoelastic Rotational Vibration Control for Remote Sensing Applications

ADAM L. WEBSTER
WILLIAM H. SEMKE
*Department of Mechanical Engineering, School of Engineering and Mines, University of North Dakota, Grand Forks, ND 58202, USA (williamsemke@mail.und.nodak.edu)*

(Received 7 September 2004; accepted 2 June 2005)

*Abstract:* The ability to eliminate, or effectively control, vibration in remote sensing applications is critical. Any perturbations of an imaging system are greatly magnified over the hundreds of kilometers from the orbiting space platform to the Earth's surface. Space platforms, such as the International Space Station, are not as predictable or stable as many other spacecraft. Therefore, an effective vibration isolation and/or absorber system is needed that operates over a wide range of excitation frequencies. A passive system is also preferred to reduce the resources required, as well as to provide a reliable and self-contained system. To accomplish these goals, a vibration amplitude limiting system has been developed that uses both vibration isolation and absorber components. Viscoelastic structural elements that act as both a spring and a damper in a single element are implemented in the design. This configuration also demonstrates a favorable frequency-dependent response and produces a system with improved dynamic behavior compared to conventional spring and damper designs. This rotation limiting vibration system has been designed and analyzed for use in digital remote sensing imaging. The transmissibility and the ground jitter associated with the system are determined. A summary of these results will be presented along with a comparison to a more conventional vibration isolation/absorber system.

*Key Words:* Vibration absorber, viscoelastic materials, passive control, remote sensing

## NOMENCLATURE

| | |
|---|---|
| $A$ | Cross-sectional area |
| $c$ | Damping coefficient |
| $c_a$ | Damping coefficient of the absorber damper |
| $c_c$ | Damping coefficient of the camera damper |
| $c_x$ | Rotational damping coefficient about the $x$-axis |
| $c_y$ | Rotational damping coefficient about the $y$-axis |
| $c_1$ | Damping coefficient of primary system |
| $c_2$ | Damping coefficient of absorber system |
| $E$ | Dynamic modulus of elasticity |
| $F_0$ | External force applied to end of beam |
| $f$ | Excitation frequency (Hz) |
| $f_s$ | Shape factor |

*Journal of Vibration and Control,* **11(11):** 1339–1356, 2005 DOI: 10.1177/1077546305057222
©2005 SAGE Publications

Downloaded from http://jvc.sagepub.com at ROCHESTER INST OF TECHNOLOGY on February 4, 2009

| | |
|---|---|
| $G$ | Dynamic modulus of rigidity |
| $h$ | Altitude of camera above imaged object |
| $I$ | Moment of inertia of cross-sectional area |
| $I_a$ | Mass moment of inertia of the absorber |
| $I_c$ | Mass moment of inertia of the camera with mount |
| $I_y$ | Moment of inertia of cross-sectional area about the $y$-axis |
| $I_1$ | Mass moment of inertia of primary system |
| $I_2$ | Mass moment of inertia of secondary system |
| $J$ | Polar moment of inertia of cross-sectional area |
| $k$ | Spring stiffness |
| $k_a$ | Stiffness of the absorber spring |
| $k_c$ | Stiffness of the camera spring |
| $k_x$ | Rotational stiffness about the $x$-axis |
| $k_y$ | Rotational stiffness about the $y$-axis |
| $k_1$ | Stiffness of primary system |
| $k_2$ | Stiffness of absorber system |
| $L$ | Line rate of line scan camera |
| $l$ | Active length of flexural joint |
| $M_0$ | External moment applied to end of beam |
| $M_y$ | External moment applied to active section of viscoelastic joint caused by rotation about the $y$-axis |
| $r$ | Distance from flexural joint to the $y$-axis |
| $T$ | Transmissibility |
| $T_a$ | Transmissibility of absorber |
| $T_c$ | Transmissibility of camera |
| $T_x$ | External torque applied to active section of viscoelastic joint caused by rotation about the $x$-axis |
| $V_z$ | External shear applied to active section of viscoelastic joint caused by rotation about the $y$-axis |
| $x$ | Position along length of beam |
| $\beta$ | Driving rotation |
| $\delta$ | Deflection |
| $\Phi$ | Rotational vibration amplitude |
| $\eta$ | Loss factor |
| $\theta$ | Angular position |
| $\theta_1$ | Angular position of primary system |
| $\theta_2$ | Angular position of secondary system |
| $\omega$ | Excitation frequency (rad $s^{-1}$) |
| $\zeta$ | Jitter of camera image |

## 1. INTRODUCTION

Remote sensing is becoming more useful in a variety of applications including precision farming practices, land management issues, disaster monitoring, and as a general data-

Downloaded from http://jvc.sagepub.com at ROCHESTER INST OF TECHNOLOGY on February 4, 2009

gathering tool. For the effective use of these systems, the ability to reduce the vibration amplitude over a wide frequency band is essential. Space platforms, such as the International Space Station (ISS), are neither completely stable nor unchanging. During the construction of the ISS many structural changes are occurring which alter its dynamic properties. The human presence also acts as a driving force in the system and the resultant motion is seen throughout the station. Therefore, a vibration limiting isolation/absorber system was needed for the remote sensing system Agricultural Camera (AgCam), being built at the University of North Dakota. AgCam will be used by the Upper Midwest Aerospace Consortium (UMAC) to assist farmers utilizing precision agriculture, which facilitates environmentally friendly farming practices, increases production, and minimizes costs.

Conventional vibration absorbers operate in a limited frequency band and are often actively controlled to adapt to various loadings. These systems have been extensively studied and implemented in a variety of applications. In specialty applications where small oscillations must be attenuated or eliminated, solution methods have been successfully demonstrated by Davis et al. (1996), Rodriquez and Perkins (1999), and Semke et al. (1998). As often is the case, the exact driving frequency is unknown or changes over time. The system developed, using frequency-dependent viscoelastic structural elements, is an effective passive method to control the transmissibility.

The use of spring–damper elements in both the absorber system and the isolator system can reduce the vibration transmissibility over a wide frequency band, as shown in Sciulli and Inman (1996) and Griffin et al. (2002). In this manner, Regelbrugge et al. (1996) have shown that efficient vibration amplitude reduction is accomplished without the cost of an active system. Furthermore, Webster and Semke (2004) have demonstrated that enhanced performance is attained with the use of frequency-dependent viscoelastic structural components.

The use of viscoelastic materials for damping and isolating structures has been studied extensively by previous researchers. Jones (2001) provides a thorough overview in his *Handbook of Viscoelastic Vibration Damping*. Several applications have been presented in conference proceedings focusing on damping and isolation (Agnes, 2002; Agnes and Wang, 2003) and on passive damping (Johnson, 1996a, 1996b). The use of a passive system for precision control of optical instruments has been implemented by Wilke et al. (1995). While these are significant accomplishments and demonstrate many benefits of utilizing viscoelastic materials, the use of a passive system to provide precision rotational isolation from broad-band excitation to produce high-quality remote sensing imagery has not been conducted.

A remote sensing camera-mounting system that utilizes vibration isolation and a vibration absorber has been designed and analyzed by Webster and Semke (2003). The system utilizes Sorbothane® viscoelastic elements that incorporate both stiffness and damping into the system. Sorbothane® exhibits stiffness and damping properties that vary non-linearly with excitation frequency. This non-linear behavior is advantageous to isolation. The material has relatively high damping at low frequencies, which allows resonant peaks to be controlled. As excitation frequency increases, the viscous damping coefficient decreases and results in better isolation at higher frequencies. It will be shown that the system is effective over a broad frequency range with reduced complexity compared to active systems with similar characteristics.

Downloaded from http://jvc.sagepub.com at ROCHESTER INST OF TECHNOLOGY on February 4, 2009

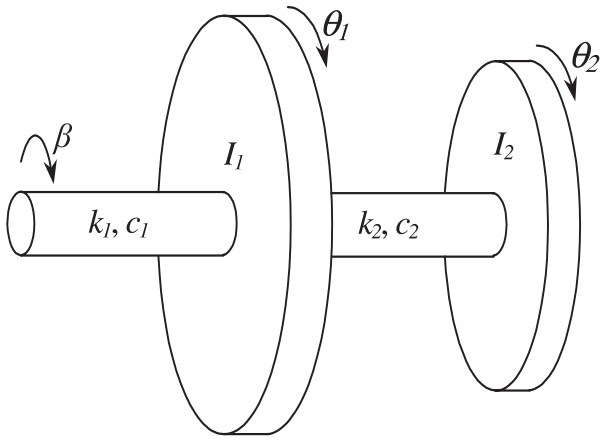


Figure 1. Rotational 2-DOF system model.

## 2. PHYSICAL MODEL FORMULATION

The vibration amplitude of a rotating system can be controlled in an analogous manner to translating systems. A simple two-degrees-of-freedom (2-DOF) rotational system is shown in Figure 1. The equations of motion of the system are

$$I_1\ddot{\theta}_1 + c_1\left(\dot{\theta}_1 - \dot{\beta}\right) + k_1\left(\theta_1 - \beta\right) + c_2\left(\dot{\theta}_1 - \dot{\theta}_2\right) + k_2\left(\theta_1 - \theta_2\right) = 0 \quad (1)$$

$$I_2\ddot{\theta}_2 + c_2\left(\dot{\theta}_2 - \dot{\theta}_1\right) + k_2\left(\theta_2 - \theta_1\right) = 0 \quad (2)$$

where $I_1$ and $I_2$ are mass moments of inertia, $k_1$ and $k_2$ are rotational stiffness, $c_1$ and $c_2$ are rotational damping constants, $\theta_1$ and $\theta_2$ are the degrees of freedom, and $\beta$ is the driving rotation. By "tuning" the physical parameters of the system, the resultant motion can be controlled. Conventional absorbers effectively isolate a single frequency well, but do not perform well over a large frequency range. However, by selectively choosing the parameters and introducing a frequency-dependent viscoelastic material, it will be shown that a broad-band frequency absorber can be produced. In the design implemented, the inertial term $I_1$ acts as the absorber and the amplitude of the inertial term $I_2$ is controlled. Therefore, the absorber acts as a tuned mount to limit the transmitted base excitations. Transmissibility ($T$) is a function of the excitation frequency $f$ and provides a measure of the effectiveness of the absorber system. It is defined as the ratio of the magnitude of the oscillation divided by the magnitude of the driving rotation:

$$T(f) = \frac{|\theta(f)|}{|\beta(f)|}. \quad (3)$$

The simple 2-DOF system illustrated the basic principles to be applied to an actual utilization of the system for broad-band viscoelastic rotational vibration control. The equations

Downloaded from http://jvc.sagepub.com at ROCHESTER INST OF TECHNOLOGY on February 4, 2009

of motion, transmissibility, and an example of a successful implementation for remote sensing applications will be shown.

## 3. REMOTE SENSING APPLICATIONS

In remote sensing applications, vibration isolation is often essential to obtain the desired image resolution with minimal distortion of the image. It is the rotational vibrations that need to be minimized for this to occur. The effects of rotational vibrations are magnified over the distance from the remote sensing platform to the object to be imaged. These distances are often hundreds of kilometers or more, so very small angular displacements can result in significant errors in the resulting image. The rotational vibration environment within the Window Observational Research Facility (WORF) to be placed aboard the ISS has not been measured, but is expected to be of frequencies of 60 Hz or less and amplitudes of 100 $\mu$rad or less. After WORF installation, the vibration testing on the ISS will be completed and the final design specifications established. The WORF provides an environment that is environmentally controlled, which eliminates large temperature variations that can greatly influence the mechanical response of viscoelastic materials. Outgassing and flammability properties are critical design considerations for use in the ISS and the Sorbothane® viscoelastic material utilized is a National Aeronautics and Space Administration (NASA) approved material that has passed all testing conducted.

Rotational behavior is a function of mass moment of inertia values rather than just mass, as in translational systems. The mass moment of inertia is dependent upon the location of mass from the axis of rotation. This fact makes it possible to create a rotational absorber with an inertia ratio greater than its mass ratio. This means that the benefits of an increased inertia ratio can be obtained with less than an equivalent increase in mass and volume. This is beneficial in nearly all situations, as it is usually desirable to minimize mass, especially in space applications.

A passive vibration control system is desired for simplicity, robustness, as well as for utilizing little or none of the limited resources available on a space mission. An active or semi-active control system requires resources such as power and computer processing time, which are often highly limited.

Incorporating the stiffness and damping elements into the system utilizing conventional metallic springs and viscous dampers poses several technical challenges such as size, mass, and mounting schemes. A solution to this problem is to use viscoelastic material as structural elements to act as isolators. Utilizing viscoelastic material reduces mass, size, and greatly simplifies mounting.

The current system utilizes line scan cameras that take in one line of pixels at a time and rely on the relative motion of the target to the camera to create a continuous digital image. The performance of a vibration isolation system on an optical payload is evaluated by examining the effect of the vibration on the resulting image. A parameter, jitter, will be introduced, which is defined as the amount of skip or overlap between consecutive lines of a line scan image. Jitter is dependent on rotational amplitude and frequency of vibration as well as the altitude and line rate of the camera. The line rate is dependent on the orbital speed of the imaging platform and the desired resolution of the image. The stiffness, damping, and

Downloaded from http://jvc.sagepub.com at ROCHESTER INST OF TECHNOLOGY on February 4, 2009

inertial properties must be chosen so that the system response is favorable over the excitation frequency range expected.

## 4. ABSORBER DESIGN

The configuration of the absorber is slightly different than those most commonly encountered in contemporary vibration texts. Rather than having the camera assembly mounted between the base and the absorber, the absorber is mounted between the camera assembly and the base. In this manner the vibration absorber component is acting as a tuned mount to limit the oscillations received by the imaging system. With appropriate parameters specified, the advantage of this configuration is recognized at frequencies above the natural frequencies of the system. The transmissibility in this range is much less than an equivalent system utilizing simple base isolation or one utilizing the conventional absorber configuration.

Incorporating the stiffness and damping elements into the system utilizing conventional metallic springs and viscous dampers posed several technical design challenges. These challenges included such things as developing an appropriate mounting scheme, as well as meeting volume and mass constraints. In this case, the solution to this problem was to incorporate viscoelastic material into the design to provide isolation as well as damping to the system. Utilizing viscoelastic material in the system resulted in a much simpler design and at the same time reduced volume and mass. Another advantage recognized when using the viscoelastic material was its beneficial frequency-dependent properties, which resulted in better performance than a system utilizing conventional spring and damper elements.

Figure 2 shows a computer aided drafting (CAD) image of the camera system mounted in the designed vibration isolation mount. The $x$- and $y$-axes of rotation are located near the bottom of the lens. The outer frame that surrounds the cameras and lens is the rotational absorber. It is designed to increase the moment of inertia about its rotational axes while minimizing added mass and volume. This is done in two ways. First, the mass is placed as far away from the rotational axis by way of the two aluminum supports along the outside of the lens. Secondly, the mass at the top of these supports is made of steel to make use of its higher density.

Primary design of the vibration absorber was to reduce vibrations about the $x$- and $y$-axes, since they will significantly affect the acquired image. Small rotations about the $z$-axis and translations in all three axes will not have significant effects on the image. Therefore, the vibration absorber is primarily designed to reduce vibrations about the $x$- and $y$-axes. However, it also isolates vibrations in the other four degrees of freedom as well.

The viscoelastic flexural joint performs the duties of both a spring and damper. In Figure 2 this joint is hidden behind the structural elements of the base, absorber, and camera mount. Figure 3 is a close-up view of the lower-right portion of the image in Figure 2. The obstructing parts have been made transparent so that the joint is visible and the active regions of the joint have been outlined.

There are two identical flexural joints in this design, one on each side of the lens. In this setup, the two joints combined perform the duties of both the absorber and camera mount isolators. The three ribs on either side of the flexural joint act as the male components in male–female fits with the aluminum structural elements. Each pair of these ribs fits into

Downloaded from http://jvc.sagepub.com at ROCHESTER INST OF TECHNOLOGY on February 4, 2009


Figure 2. CAD image of camera and absorber with rotation axes.

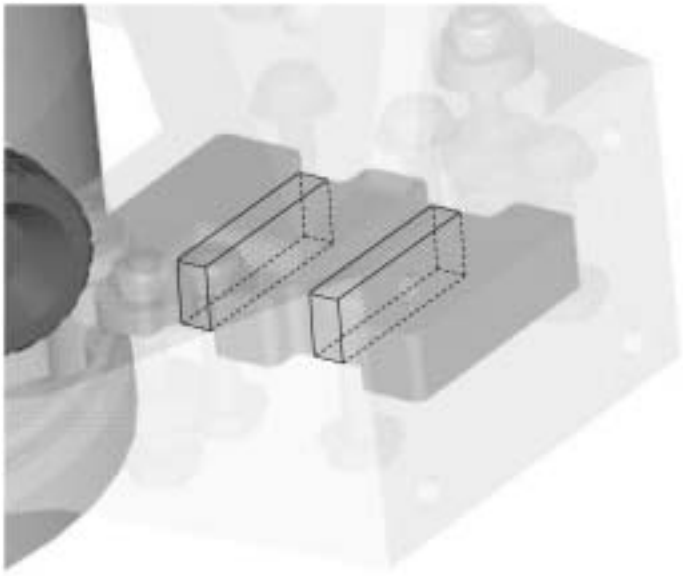

Figure 3. Detailed view of viscoelastic flexural joint.

Downloaded from http://jvc.sagepub.com at ROCHESTER INST OF TECHNOLOGY on February 4, 2009

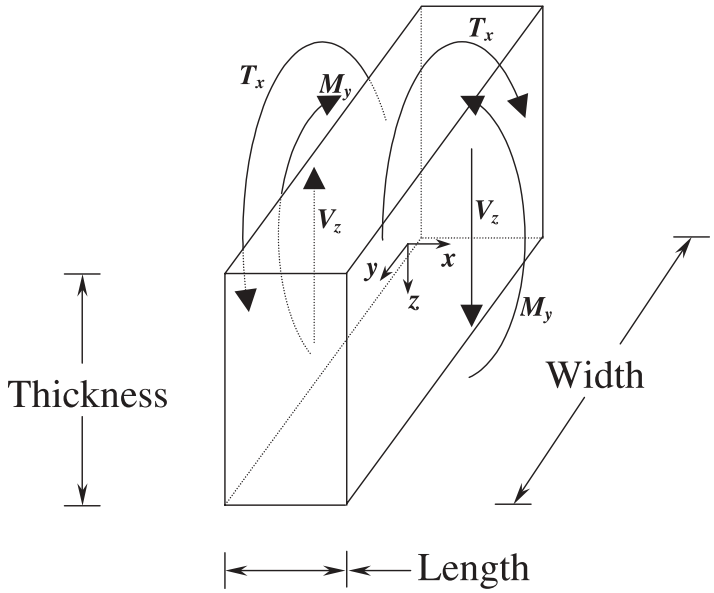


Figure 4. Schematic diagram of active section of viscoelastic joint.

Table 1. Dimensions of active portions of flexural joint.

| Dimension | Absorber isolator | Camera isolator |
|---|---|---|
| Width | 31.75 mm | 31.75 mm |
| Length | 12.7 mm | 6.35 mm |
| Thickness | 4.76 mm | 4.76 mm |
| Distance from $y$-axis | 101.2 mm | 76.2 mm |

one of the three structural elements: the base, the absorber, and the camera assembly. The thinner sections between the ribs are the portions that will deform under rotation, the active sections, to perform the duties of the spring and damper. Figure 4 shows a schematic diagram of the loads applied on the active sections of the flexural joint under rotational displacements about the $x$- and $y$-axes. The external loads applied are a moment ($M_y$), a shear force ($V_z$), and a torque ($T_x$). The effective dimensions of the isolators are shown in Table 1. These dimensions were chosen to provide sufficient performance as well as to fit into the available space in the design.

## 5. VISCOELASTIC MODELING

Viscoelastic materials have other aspects that make them desirable alternatives to conventional methods of vibration isolation. One of these aspects is how the dynamic stiffness and damping properties vary with excitation frequency. Both of these characteristics have a nonlinear dependence on the excitation frequency. The most beneficial aspect of this dependence

Downloaded from http://jvc.sagepub.com at ROCHESTER INST OF TECHNOLOGY on February 4, 2009

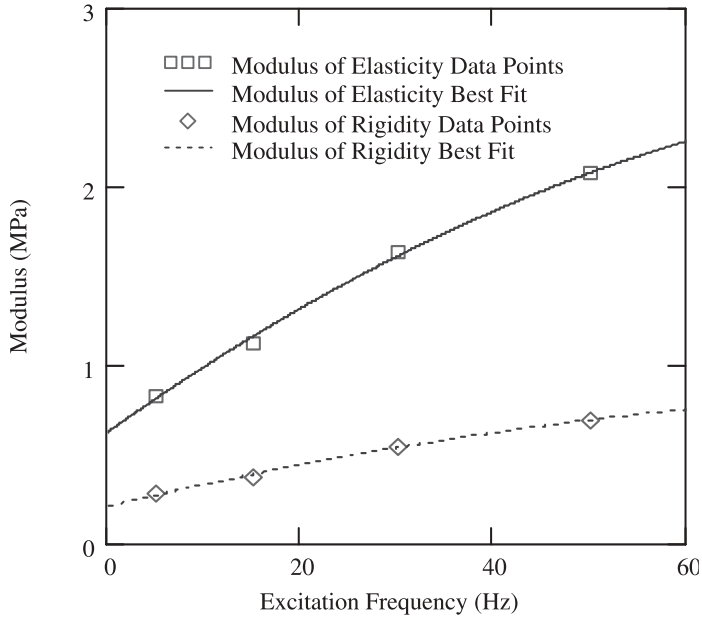


Figure 5. Dynamic modulus versus excitation frequency.

is the decrease in damping at higher frequencies. With a properly designed system, this property allows for effective damping at the resonant frequencies and as the excitation frequency increases the damping decreases. A large damping coefficient is often needed to control amplitudes at resonance, but increasing the damping coefficient results in higher transmissibility at higher frequencies. In a system utilizing conventional damping, the damping coefficient is constant, which results in a trade-off between low- and high-frequency performance. Therefore, utilizing viscoelastic material that has reduced damping at increased frequencies results in better isolation at the higher frequencies than a comparable system with a constant damping coefficient.

The damping coefficient is inversely proportional to excitation frequency. However, both the loss factor and the spring stiffness are non-linearly dependent on frequency, so the damping coefficient also has a non-linear dependency upon frequency. In the analysis, small displacements were assumed so that the damping is modeled with a linear relationship between damping force and angular velocity for a given excitation frequency. It was also assumed that over this small displacement range the dynamic stress–strain relationship is approximately linear.

In order to model the behavior of the viscoelastic material over an entire frequency range, continuous curves are needed for the dynamic stiffness and loss factor properties of the material. The method of least-squares was used to fit second-order polynomials to the dynamic modulus of elasticity, the dynamic modulus of rigidity, and loss factor data from product data sheets for durometer 70 Sorbothane® at 23°C. The loss factor is a dimensionless parameter that is used to represent the relative amount of internal damping of a material. Figure 5 shows the supplied data points and the least-squares fits for the dynamic modulus of elasticity and

Downloaded from http://jvc.sagepub.com at ROCHESTER INST OF TECHNOLOGY on February 4, 2009

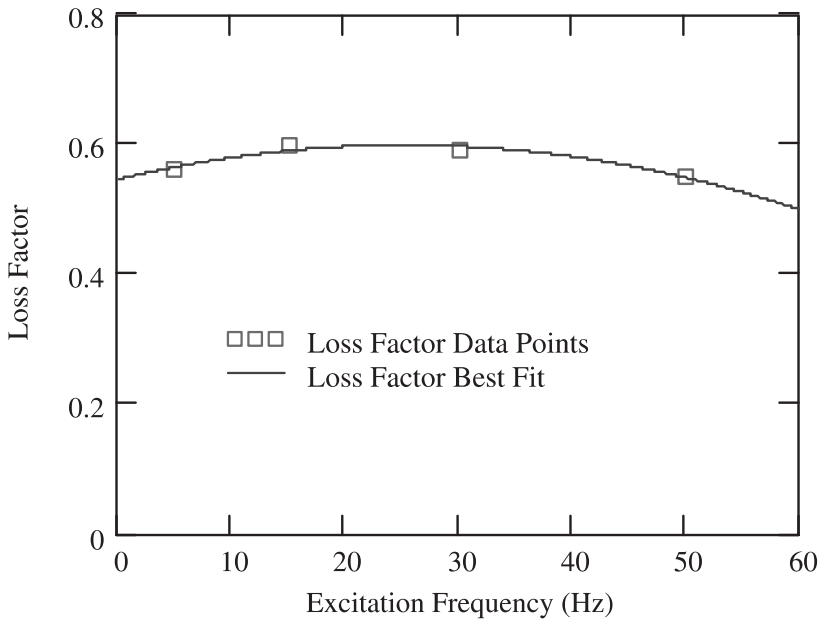


Figure 6. Loss factor versus excitation frequency.

dynamic modulus of rigidity. Figure 6 shows the supplied data points and least-squares fit for the loss factor. Equations (4) and (5) show the second-order least-squares fit polynomials used to model the dynamic modulus of elasticity ($E$) and dynamic modulus of rigidity ($G$), respectively. The input into these equations is the excitation frequency in Hz and the output is the dynamic modulus in MPa. Equation (6) shows the polynomial used to model the loss factor ($\eta$). Again, the input of this equation is the excitation frequency in Hz; the output is the dimensionless loss factor parameter.

$$E(f) = -0.0001892\,f^2 + 0.0385\,f + 0.6207 \quad (4)$$

$$G(f) = -0.00006307\,f^2 + 0.0128\,f + 0.2069 \quad (5)$$

$$\eta(f) = -0.0000828\,f^2 + 0.004191\,f + 0.5458 \quad (6)$$

## 6. STIFFNESS AND DAMPING DERIVATION

The flexural joint isolates the camera from vibrations in all six degrees of freedom. The primary design emphasis was placed on decreasing rotations about the $x$- and $y$-axes because rotations in these two axes have the most significant detrimental effects on the image from the camera. In order to determine the performance in these two degrees of freedom, the appropriate stiffness and damping parameters are determined for the flexure joint.

The design of the viscoelastic flexure joint basically consists of a beam, which relies on two separate uncoupled modes of deflection to accommodate the two axes of rotation. In

Downloaded from http://jvc.sagepub.com at ROCHESTER INST OF TECHNOLOGY on February 4, 2009

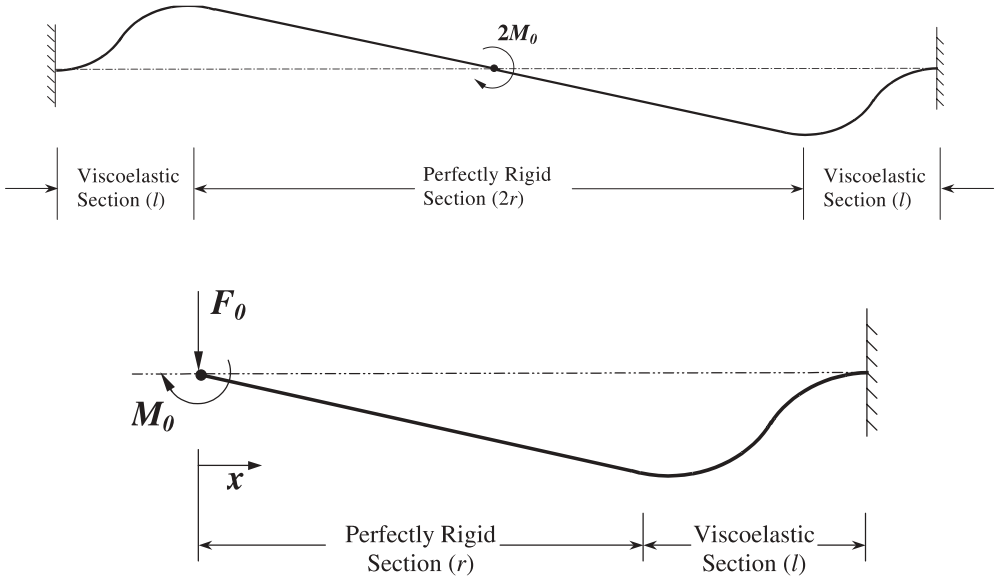


Figure 7. Schematics of the deflection mode of the viscoelastic joints and the simplified deflection mode using antisymmetry.

each case, the ends of the flexural joint were assumed to act as a cantilever. The stiffness about the $x$-axis relies on the torsional stiffness and was determined using the simple angular deflection formula for torsion. The resulting stiffness ($k_x$) is given by

$$k_x = \frac{2GJ}{l} \tag{7}$$

where $J$ is the polar moment of inertia of the cross-section and $l$ is the active length of the flexural joint.

The equation modeling the rotational stiffness of the joint about the $y$-axis was determined using an energy method. The mode of deflection in the case of rotation about the $y$-axis is represented by the schematics in Figure 7. The design of the joint is two viscoelastic structural elements mounted between a fixed base and the aluminum bracket, which is rigidly attached to the imaging system. The viscoelastic joints provide stiffness due to bending and shear. The joint is essentially a short beam so the shear effects are not negligible and classic beam theory is not applicable. In this analysis, the ends of the viscoelastic springs attached to the base are considered fixed. The stiffness of the center aluminum section has a bending stiffness value ($EI$) that is more than five orders of magnitude greater than that of the viscoelastic joints. So, any deflection of the aluminum structure is negligible compared to the deflections of the viscoelastic joints. Therefore, the aluminum structure was treated as if it was perfectly rigid compared to the viscoelastic material.

The deflection analysis can be simplified by noting that there is antisymmetry in this system. The first schematic in Figure 7 can then be simplified to the second schematic. The simplified system has two loadings to provide the appropriate boundary conditions: a

Downloaded from http://jvc.sagepub.com at ROCHESTER INST OF TECHNOLOGY on February 4, 2009

downward force ($F_0$) applied at $x = 0$ and a clockwise moment ($M_0$) applied at $x = 0$. The deflected shapes of the beam when subjected to these two load cases were found individually. The deflections of the two component load cases are both linear so they can simply be added together using the principle of superposition.

To include the shear effects into the analysis, an energy method was used. The total internal strain energy in the beam was determined. This included energy due to the transverse shear and the internal moment in the beam. In the case of the transverse shear energy, a shape factor ($f_s$), was calculated based on the cross-sectional shape of the beam. The shape factor is a dimensionless parameter and for a beam of rectangular cross section equal to 1.2 (Hibbeler, 1997).

The total internal energy was then used with Castigliano's theorem to derive mathematical functions of the deflection and slope of the beam due to the applied moment. One of the requirements to use Castigliano's theorem is that the material have a linear stress–strain relationship (Shigley and Mischke, 1989). It was assumed that the material behaved approximately linearly in the range of the small deflections that would be encountered. This assumption is also critical in the use of the principle of superposition. The deflection and slope were determined in a piecewise manner, with one equation for the rigid section and a separate equation for the viscoelastic section. The rigid section is represented by the interval of $0 = x = r$, and the viscoelastic region is represented by the interval of $r = x = r + l$. Equations (8) and (9) show the deflection and slope of the beam, respectively:

$$\delta = \begin{cases} \dfrac{M_0 l}{EI}\left(r + \dfrac{1}{2}l - x\right) - \dfrac{f_s l F_0}{GA} - \dfrac{F_0}{2EI}\left[\dfrac{2}{3}\left((r+l)^3 - r^3\right) + \left(r^2 - (r+l)^2\right)x\right] \\ \qquad 0 \le x \le r \\ \dfrac{M_0}{EI}\left[\dfrac{1}{2}x^2 + \dfrac{1}{2}(r+l)^2 - (r+l)\,x\right] - \dfrac{f_s F_0\,(r+l-x)}{GA} \\ \qquad - \dfrac{F_0}{2EI}\left[\dfrac{2}{3}\left((r+l)^3 - x^3\right) + \left(x^2 - (r+l)^2\right)x\right] \qquad r \le x \le r + l \end{cases} \tag{8}$$

$$\theta = \begin{cases} -\dfrac{M_0 l}{EI} + \dfrac{F_0}{2EI}\left((r+l)^2 - r^2\right) & 0 \le x \le r \\ -\dfrac{M_0}{EI}(r + l - x) + \dfrac{f_s F_0}{GA} + \dfrac{F_0}{2EI}\left((r+l)^2 - x^2\right) & r \le x \le r + l \end{cases}. \tag{9}$$

The force ($F_0$) exerted on the beam and the moment ($M_0$) applied to the beam are coupled together, meaning that they are not independent of each other. The relationship between $F_0$ and $M_0$ is found by using the deflection function previously derived and evaluating it at the boundary condition $\delta(0) = 0$ (deflection at the position $x = 0$ is equal to zero). The relationship between $F_0$ and $M_0$ is

$$F_0 = M_0 \frac{GA\left(r + \dfrac{1}{2}l\right)}{f_s EI + GA\left(r^2 + rl + \dfrac{1}{3}l^2\right)}. \tag{10}$$

Downloaded from http://jvc.sagepub.com at ROCHESTER INST OF TECHNOLOGY on February 4, 2009

The rigid portion of the slope equation is of primary concern because it defines the actual rotation of the camera. From this equation the equivalent rotational spring constants for the $y$-axis can be found. The $y$-axis spring constant is shown in equation (11). Recall that the dynamic modulus of elasticity ($E$) and the dynamic modulus of rigidity ($G$) are frequency-dependent. So, in turn, the rotational stiffness is also frequency-dependent:

$$k_y = \frac{2EI_y}{l}\left[\frac{f_s EI_y + GA\left(r^2 + rl + \frac{1}{3}l^2\right)}{f_s EI_y + \frac{1}{12}GAl^2}\right]. \tag{11}$$

The Kelvin–Voigt model was used to model the damping coefficient of the viscoelastic material, as described in Inman (2001). This model states that the damping coefficient is dependent on the excitation frequency, the stiffness, and the loss factor as shown in equation (12). The stiffness and loss factor are both dependent on the excitation frequency; therefore, the damping coefficient is a function of the excitation frequency. The damping components for the $x$- and $y$-axes ($c_x$, $c_y$) are found in equations (13) and (14), respectively

$$c = \frac{\eta k}{\omega} \tag{12}$$

$$c_x = \frac{2\eta GJ}{\omega l} \tag{13}$$

$$c_y = \frac{2\eta EI_y}{\omega l}\left[\frac{f_s EI_y + GA\left(r^2 + rl + \frac{1}{3}l^2\right)}{f_s EI_y + \frac{1}{12}GAl^2}\right] \tag{14}$$

where $\omega$ is the excitation frequency in rad s$^{-1}$.

## 7. EVALUATION OF PERFORMANCE

An analysis was performed based on the application of a harmonic sinusoidal input to the system. The transmissibilities of the absorber and camera ($T_a$, $T_c$) under this input are

$$T_a = \left(\frac{\left[k_a k_c - (k_a I_c + c_a c_c)\omega^2\right]^2 + \left[(k_a c_c + k_c c_a)\omega - c_a I_c \omega^3\right]^2}{\left[I_a I_c \omega^4 - (c_a c_c + I_c(k_a + k_c) + k_c I_a)\omega^2 + k_a k_c\right]^2 + \left[(k_a c_c + k_c c_a)\omega - (c_a I_c + c_c(I_a + I_c))\omega^3\right]^2}\right)^{\frac{1}{2}} \tag{15}$$

$$T_c = \left(\frac{\left[k_a k_c - c_a c_c \omega^2\right]^2 + \left[(k_a c_c + k_c c_a)\omega\right]^2}{\left[I_a I_c \omega^4 - (c_a c_c + I_c(k_a + k_c) + k_c I_a)\omega^2 + k_a k_c\right]^2 + \left[(k_a c_c + k_c c_a)\omega - (c_a I_c + c_c(I_a + I_c))\omega^3\right]^2}\right)^{\frac{1}{2}} \tag{16}$$

where the subscripts $a$ and $c$ refer to the absorber and camera, respectively.

Graphs of the transmissibility of the absorber and camera assembly are shown in Figures 8 and 9. These curves are based on the stiffness, damping, and inertia values for the

Downloaded from http://jvc.sagepub.com at ROCHESTER INST OF TECHNOLOGY on February 4, 2009

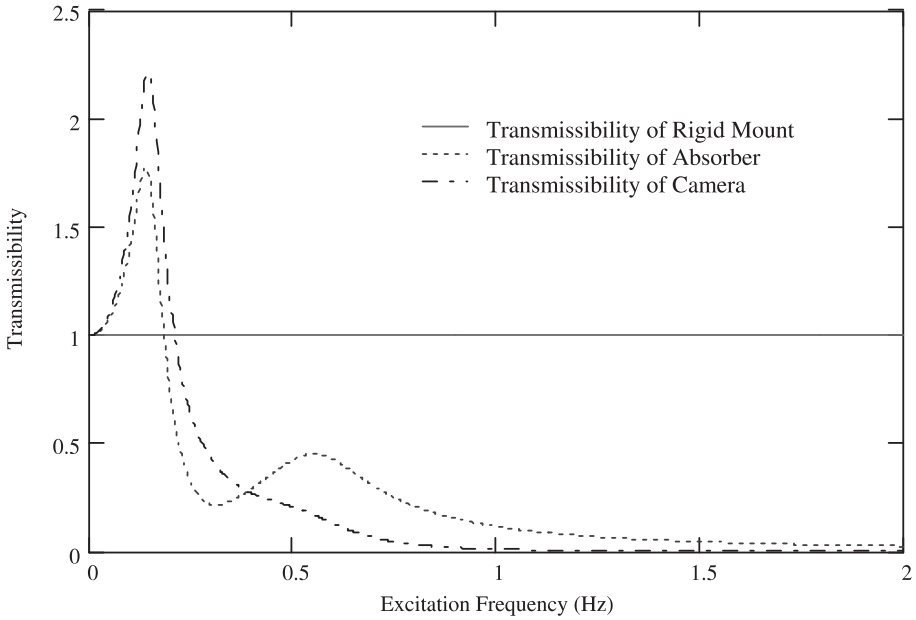


Figure 8. The *x*-axis transmissibility versus excitation frequency for the absorber and camera assembly.

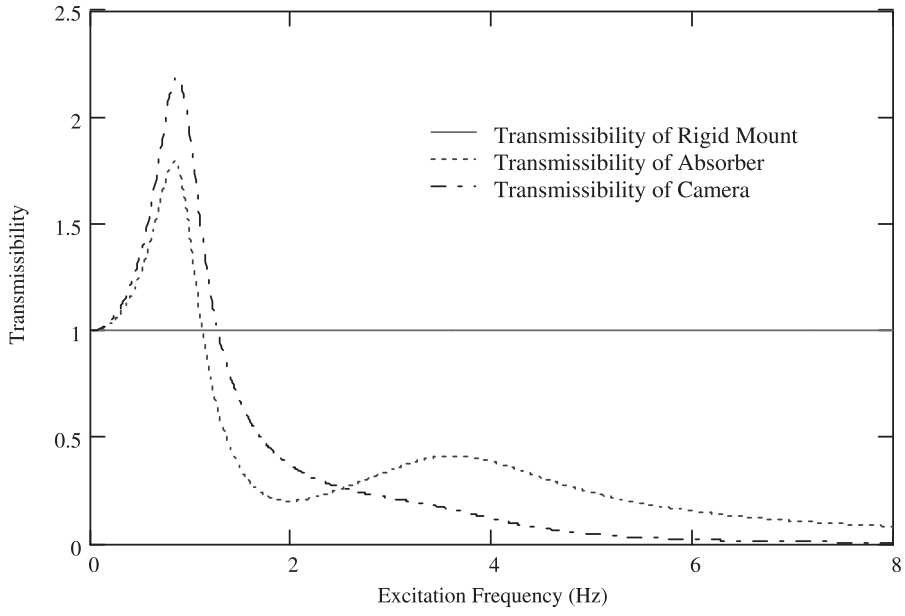


Figure 9. The *y*-axis transmissibility versus excitation frequency for the absorber and camera assembly.

Downloaded from http://jvc.sagepub.com at ROCHESTER INST OF TECHNOLOGY on February 4, 2009

Table 2. Mass moment of inertia values.

| Rotation axis | $x$-axis | $y$-axis |
|---|---|---|
| Absorber inertia (kg m$^2$) | 0.1463 | 0.1610 |
| Camera assembly inertia (kg m$^2$) | 0.2926 | 0.3219 |

motion about the $x$- and $y$-axes, respectively. The mass moment of inertia values about the $x$- and $y$-axes are shown in Table 2. The transmissibilities are compared to the case of a rigid mount in which the transmissibility is constant and equal to 1. In order to see clearly the behavior of the system at resonance, the graph shows only a limited range. There is little to be inferred at frequencies above these ranges because the transmissibility of both the absorber and camera assembly asymptotically approach zero. The amplitudes in each direction are similar; however, the peak frequencies are different. This occurs because the stiffness in the two orthogonal directions is not the same due to the geometry of the flexural joints. The two orthogonal directions could be made to have identical transmissibilities, but were not due to geometric constraints and the success at meeting the desired performance levels.

A good way to evaluate the performance of a vibration isolation system on an optical payload is to examine the effect of the vibration on the resulting image. To do this, a new parameter called jitter ($\zeta$) is introduced. Jitter is defined as the amount of skip or overlap between consecutive lines of a line scan image. A line scan camera is a digital camera that "builds" a cohesive image by taking one line of pixels of the image at a time and relying on the relative motion of the camera to the imaged object to create a continuous picture. Excessive jitter will result in an image in which consecutive lines do not correctly match up, and it may contain skips and overlaps. Jitter is a function of the amplitude and frequency of vibration, the altitude of the imaging platform, and the line rate of the camera. The latter parameter is dependent on the desired pixel resolution of the image and the ground track velocity. Equation (17) defines the jitter expected with the absorber system in place:

$$\zeta = \frac{\Phi \omega h}{L} \left( \frac{\left[k_a k_c - (k_a I_c + c_a c_c)\omega^2\right]^2 + \left[(k_a c_c + k_c c_a)\omega - c_a I_c \omega^3\right]^2}{\left[I_a I_c \omega^4 - (c_a c_c + I_c(k_a + k_c) + k_c I_a)\omega^2 + k_a k_c\right]^2 + \left[(k_a c_c + k_c c_a)\omega - (c_a I_c + c_c(I_a + I_c))\omega^3\right]^2} \right)^{\frac{1}{2}}. \tag{17}$$

Figure 10 shows a graph comparing the level of jitter with no isolation to the predicted jitter with isolation. These curves were formed using the parameters in Table 3 and the inertia values in Table 2. The predicted behavior with isolation is provided for both the $x$- and $y$-axes. Due to physical parameters of the flexural joint and camera assembly, the jitter about the two axes is different. The parameters are governed by commercial availability along with space and manufacturing requirements to attain the desired performance, the primary objective. To put the results in perspective, it is informative to look at the desired image resolution. In this case, the desired image resolution was 10 m, meaning each pixel of the image covers 10 m on the ground. As can be seen from the graph, the maximum predicted jitter is less than 0.7 m, or less than 7% of one pixel.

The 7% jitter performance level was deemed highly acceptable by end-users who utilize the images. A maximum allowable jitter was set at 2 m or 20% of the pixel size. Without isolation, jitter increases linearly with frequency and tends towards infinity. At frequencies

Downloaded from http://jvc.sagepub.com at ROCHESTER INST OF TECHNOLOGY on February 4, 2009

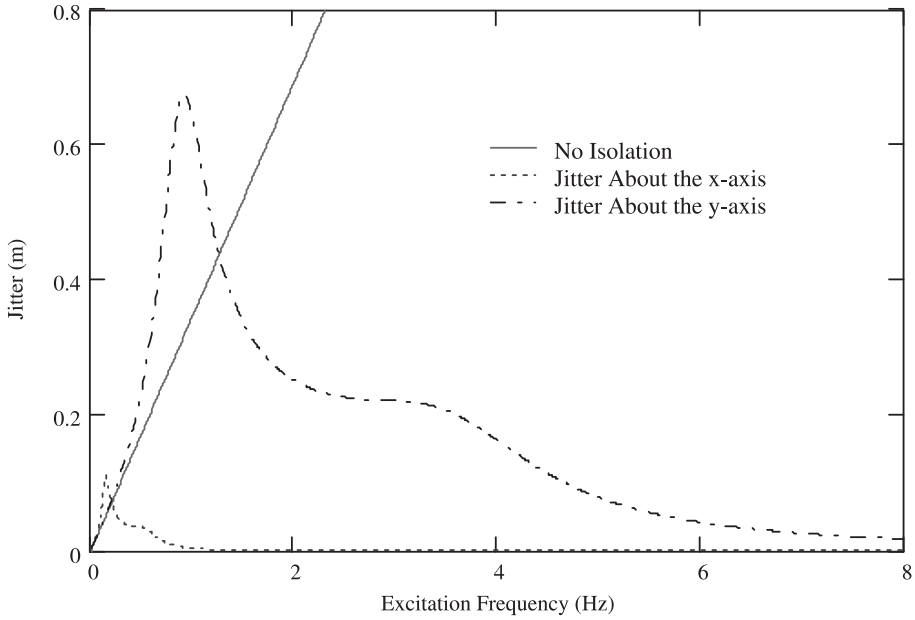


Figure 10. Jitter versus excitation frequency for the *x*- and *y*-axes.

Table 3. Jitter parameters.

| | |
|---|---|
| Amplitude of rotational vibration ($\Phi$) | 100 $\mu$rad |
| Altitude of imaging platform ($h$) | 400 km |
| Line rate ($L$) | 725 Hz |

above 6 Hz it fails to meet the maximum allowable level. The absorber system designed has improved performance over an isolation only system and is advantageous for the success of the mission.

## 8. SUMMARY OF RESULTS

The rotational, two-axis vibration absorber designed has been predicted to perform adequately in its role of reducing vibrations felt by the camera. The viscoelastic flexural joints simplify mechanical design and exhibit frequency-dependent properties that are beneficial to vibration isolation. Figure 11 shows the percent improvement in transmissibility of a viscoelastic design over a system utilizing conventional springs and damping elements. In this comparison the parameters of the conventional system were set such that the frequency and magnitude of the resonant peaks of the two systems coincide. It can be seen that at the low frequencies near the resonant peak there is minimal improvement using the viscoelastic material. At frequencies above the resonant peak the improvement is dramatic, approaching 100%. At the lower frequencies the performance is actually below that of conventional sys-

Downloaded from http://jvc.sagepub.com at ROCHESTER INST OF TECHNOLOGY on February 4, 2009

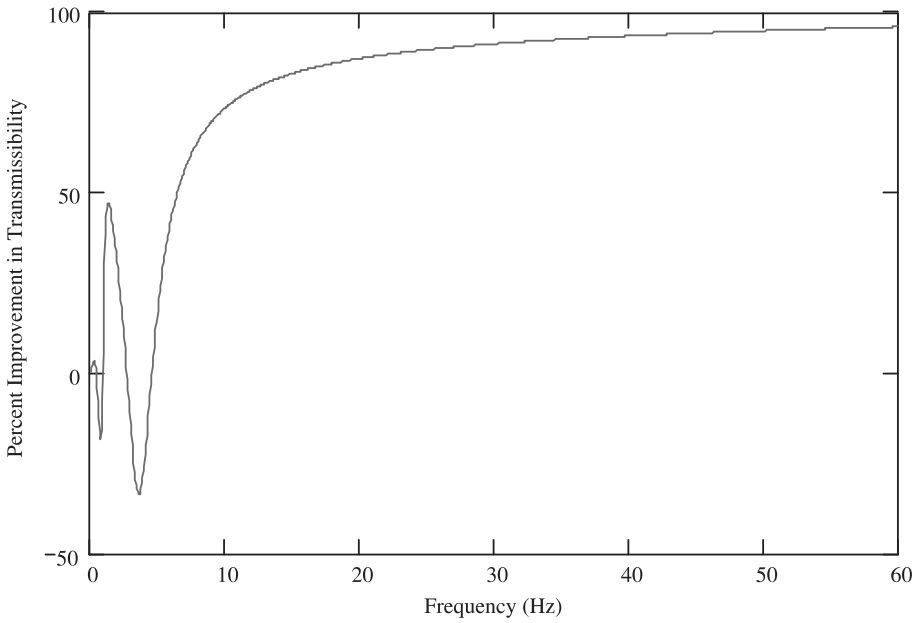


Figure 11. Percent improvement in transmissibility of a viscoelastic absorber system over an absorber utilizing conventional components.

tems at times, but jitter is not a significant issue at the lower frequencies as it is at the higher frequencies. Therefore, the enhanced performance due to the frequency-dependent materials is beneficial to meet the stringent demands of the remote sensing system. The broad-band effectiveness is also critical due to the limited knowledge of the dynamic behavior of the WORF rack on the ISS.

It is useful to note that this absorber system is designed for use on a space-based platform in a zero-gravity environment. Under normal gravitational conditions, the static deflections due to the weight of the system would be too great for the flexural joint to support.

## 9. CONCLUSIONS

An effective rotational vibration absorption and isolation system has been designed and analyzed for use in space borne remote sensing. The system is capable of supporting a digital camera system in a manner such that the jitter in the images is under 7%, thus meeting the needs of the scientific community. This broad frequency band, passive system is made possible by tuning the physical parameters of the system and implementing viscoelastic materials. The system is also passive, which reduces the complexity, cost, and resources active systems require. The system also demonstrates improved performance over nearly the entire anticipated operational range. The system is robust, economical, and performs well. Thus, it will be utilized by the University of North Dakota AgCam system to enable high-quality imaging for the farmers and ranchers of this region and around the world.

Downloaded from http://jvc.sagepub.com at ROCHESTER INST OF TECHNOLOGY on February 4, 2009

*Acknowledgment. This research was supported in part by NASA Grant NAG13-01006, "Northern Great Plains Center for People and the Environment".*

## REFERENCES

Agnes, G., ed., 2002, "Smart structures and materials 2002 – damping and isolation," *Proceedings of SPIE* **4697**.

Agnes, G. and Wang, K., eds., 2003, "Smart structures and materials 2003 – damping and isolation," *Proceedings of SPIE* **5052**.

Davis, T., Davis, P., Sullivan, J., Hoffman, T., and Das, A., 1996, "High performance passive viscous isolator element for active/passive (hybrid) isolation," *Proceedings of SPIE* **2720**, 281–292.

Griffin, S., Gussy, J., Lane, S., Henderson, B., and Sciulli, D., 2002, "Virtual skyhook vibration isolation system," *ASME Journal of Vibration and Acoustics*, **124**, 63–67.

Hibbeler, R. C., 1997, *Mechanics of Materials*, 3rd edn, Prentice-Hall, Upper Saddle River, NJ.

Inman, D., 2001, *Engineering Vibration*, 2nd edn, Prentice-Hall, Englewood Cliffs, NJ.

Johnson, C., ed., 1996a, "Smart structures and materials 1995 – passive damping," *Proceedings of SPIE* **2445**.

Johnson, C., ed., 1996b, "Smart structures and materials 1996 – passive damping and isolation," *Proceedings of SPIE* **2720**.

Jones, D., 2001, *Handbook of Viscoelastic Vibration Damping*, Wiley, New York.

Regelbrugge, M., Carrier, A., and Dickson, W., 1996, "Performance of a smart vibration isolator for precision spacecraft instruments," *Journal of Intelligent Material Systems and Structures* **7**, 211–215.

Rodriquez, H. and Perkins, B., 1999, "Feasibility study on low-frequency passive vibration isolation for the international standard payload rack," *American Institute of Aeronautics and Astronautics* 2, 887–893.

Sciulli, D. and Inman, D., 1996 "Comparison of single- and two-degree-of-freedom models for passive and active vibration isolation design," *Proceedings of SPIE* **2720**, 293–304.

Semke, W., Engelstad, R., Lovell, E., and Liddle, J., 1998, "Dynamic analysis of a SCALPEL mask during electron beam exposure," *Journal of Vacuum Science and Technology B* **16(6)**, 3587–3591.

Shigley, J. and Mischke, C., 1989, *Mechanical Engineering Design*, 5th edn, McGraw-Hill, New York.

Webster, A. and Semke, W., 2003, "Viscoelastic rotational vibration absorber for remote sensing applications," in *Proceedings of ASME Design and Engineering Technical Conference*, Chicago, IL.

Webster, A. and Semke, W., 2004, "Frequency-dependent viscoelastic structural elements for passive broad-band vibration control," *Journal of Vibration Control* **10(6)**, 881–895.

Wilke, P., Decker, T., and Hale, L., 1995, "Highly damped exactly constrained mounting of an X-ray telescope," *Proceedings of SPIE* **2445**, 2–13.

Downloaded from http://jvc.sagepub.com at ROCHESTER INST OF TECHNOLOGY on February 4, 2009